Flux melting in BSCCO: Incorporating both electromagnetic and Josephson couplings

Sandeep Tyagi and Yadin Y. Goldschmidt

Department of Physics and Astronomy,

University of Pittsburgh, Pittsburgh, Pennsylvania 15260

Abstract

Multilevel Monte Carlo simulations of a BSCCO system are carried out including both Josephson as well as electromagnetic couplings for a range of anisotropies. A first order melting transition of the flux lattice is seen on increasing the temperature and/or the magnetic field. The phase diagram for BSCCO is obtained for different values of the anisotropy parameter γ. The best fit to the experimental results of D. Majer *et al.* [Phys. Rev. Lett. **75**, 1166 (1995)] is obtained for $\gamma \approx 250$ provided one assumes a temperature dependence $\lambda^2(0)/\lambda^2(T) = 1-t$ of the penetration depth with $t = T/T_c$. Assuming a dependence $\lambda^2(0)/\lambda^2(T) = 1 - t^2$ the best fit is obtained for $\gamma \approx 450$. For finite anisotropy the data is shown to collapse on a straight line when plotted in dimensionless units which shows that the melting transition can be satisfied with a single Lindemann parameter whose value is about 0.3. A different scaling applies to the $\gamma = \infty$ case. The energy jump is measured across the transition and for large values of γ it is found to increase with increasing anisotropy and to decrease with increasing magnetic field. For infinite anisotropy we see a 2D behavior of flux droplets with a transition taking place at a temperature independent of the magnetic field. We also show that for smaller values of anisotropy it is reasonable to replace the electromagnetic coupling with an in-plane interaction represented by a Bessel function of the second kind (K_0), thus justifying our claim in a previous paper.

I. INTRODUCTION

High-temperature superconductors are materials of type II, that allow for partial magnetic flux penetration if the external field satisfies $H_{c1} < H < H_{c2}$[1,2,3]. The flux penetrates the sample in the form of flux-lines (FL's), each containing a quantum unit $\phi_0 = hc/2e$ of flux. At low temperature the FL's form an ordered hexagonal lattice (Abrikosov lattice) due to their their mutual repulsion. The lattice constant is given by $a_0 = \sqrt{2\phi_0/\sqrt{3}B}$, where B is the magnetic field flux density. At high temperature and/or magnetic field this lattice melts due to thermal fluctuations[4,5,6,7,8]. Two of the most commonly used high-temperature superconductors are $YBa_2Cu_3O_{7-\delta}$ (YBCO) and $Bi_2Sr_2CaCu_2O_{8+\delta}$ (BSCCO). They are very different in one very important respect - their anisotropy parameter γ, defined as $\gamma^2 = m_z/m_\perp$, where m_z and $m_\perp$ denote the effective masses of electrons moving along the c axis and the ab plane, respectively. While for YBCO the anisotropy is somewhere between 5-7, for BSCCO it is estimated to be between 10 to a 100 times larger, and estimates vary across the literature. What contributes to the discrepancy of different estimates is the fact that the anisotropy varies depending on the degree of doping. There is also the question of how to extract the value of anisotropy correctly from the exerimental results. Blatter *et al*[2] cite a range of anisotropies of 50-200 for BSCCO. References [7,9,10] cite values in the range of 140-160. However more recent acurate measurements[11] the components of the London penetration depths λ_c and λ_{ab}, the ratio of which is γ, are consistent with anisotropy in the range of 300-500 for optimally doped samples. The previously reported lower values may belong to overdoped samples or constituted only a lower bound. Anisotropy controls the amount of "wiggling" of a flux-line from plane to plane. In YBCO the FL's are more rigid while in BSCCO they are so loose that they are customarily referred to as a stack of two dimensional pancakes[12] (or droplet vortices) rather than FL's.

Interaction between two FL's in YBCO is non-local. It is a screened Bio-Savart type of interaction where each segment of a FL interacts with every other segment of the same FL and all the other FL's. For segments oriented in the same direction the interaction is repulsive[2]:

$$\mathcal{F} = \frac{\varepsilon_0}{2} \sum_{ij} \int d\mathbf{s}_i(z) \cdot d\mathbf{s}_j(z') \frac{\exp(-|\mathbf{s}_i(z) - \mathbf{s}_j(z')|/\lambda)}{|\mathbf{s}_i(z) - \mathbf{s}_j(z')|} \tag{1.1}$$

Here $\mathbf{s}_i(z)$ denotes the position of the i'th FL at elevation z along the z-axis, $\varepsilon_0 = \phi_0^2/(4\pi\lambda)^2$

is the line energy and λ is the screening length (penetration depth). Considering two given FL's, it turns out though that it is a good approximation to replace the non-local interaction of a given line segment of one FL, with all segments of the other FL with a single interaction among segments belonging to the same plane. This interaction is given approximately by[13] $2\,\varepsilon_0\,d\,K_0(R_{ij}/\lambda)$ where R_{ij} is the distance between the two segments in the same plane and d is the thickness of each layer. The approximation is valid when the FL's do not deviate too much from straight lines which is a good approximation for YBCO in the "solid" vortex lattice phase, because FL's are stiff and do not wiggle too much. For each FL, there is also an elastic energy associated with its deviation from a straight line along the z-direction. The elastic energy of a flux-line in YBCO is approximately given by

$$\frac{\epsilon_l}{2}\int_0^L dz\,(d\mathbf{R}(z)/dz)^2, \tag{1.2}$$

assuming the external magnetic field is aligned along the z-direction. The elastic coefficient (line tension) ϵ_l is equal to $\varepsilon_0\,\ln(\lambda/\xi)/\gamma^2$ where ξ is the coherence length, and γ is the anisotropy. In the discrete case this self-energy transforms into an attractive quadratic interaction between segments in adjacent planes. In this form the problem is equivalent to a system of bosons with repulsive interactions[13,14]. The term described in the last equation corresponds to the kinetic energy of the bosons which repel each other with a screened Coulomb interaction.

For BSCCO the situation is different because each FL is represented more faithfully by a collection of pancakes. Each pancake interacts with every other pancake, but the interaction is different from the interaction among FL segments discussed above. The interaction can be shown to consist of two parts. The first part is called the electromagnetic interaction (or simply magnetic) and it exists even in the case that the layers of the materials are completely decoupled, so no current can flow along the c-axis of the sample. A pancake vortex located in one plane gives rise to screening currents in the same plane as well as in all other planes. A second pancake vortex, located elsewhere, interacts with the screening currents induced by the first pancake[15]. This interaction has been calculated by Clem and others[12]. Two pancakes in the same plane interact with a repulsive interaction while pancakes in different planes attract one another. If one considers a single pancake vortex and an infinite set of pancakes a distance R away stacked along the z-axis, then the interaction still sums to $2\,\varepsilon_0\,d\,K_0(R/\lambda)$ in the limit when d/λ goes to zero (see Appendix A). Clem[12] proceeds to

show that if one has a straight array of pancake vortices along the z-axis, and one pancake of the stack is displaced a distance R in the lateral direction then the magnetic energy of the configuration increases by an amount

$$\Delta E(R) = \frac{{d\phi_0}^2}{8\pi^2\lambda^2}\left(\mathcal{C} + \ln\left(\frac{R}{2\lambda}\right) + K_0\left(\frac{R}{\lambda}\right)\right). \tag{1.3}$$

where $\mathcal{C}$ is Euler's constant (=0.5772...). For large R ($R \gg \lambda$), the modified Bessel function K_0 decays exponentially and thus the energy increases like $\ln(R/\lambda)$. For small R the Bessel function can be expanded in a power series in R/λ

$$K_0(R/\lambda) = -\ln(R/2\lambda)(1 + R^2/4\lambda^2 + \cdots) - \mathcal{C} + R^2(1-\mathcal{C})/4\lambda^2 + \cdots, \tag{1.4}$$

and thus the electromagnetic energy behaves like R^2 to leading order in R.

The second part of the interaction among pancake vortices is the so-called Josephson interaction[2,15,16]. It results from the fact that there is a Josephson current flowing between two superconductors separated by an insulator and this current is proportional to the sine of the phase difference of the superconducting wave functions. The superconductors in the present case are the different CuO_2 planes. When two pancakes belonging to the same stack and residing in adjacent planes move away from each other, the phase difference that originates causes a Josephson current to begin flowing between the planes. This results in an attractive interaction between pancakes that for distances small compared to $r_g \equiv \gamma d$ is approximately quadratic[2,15] in the distance. When the two adjacent pancakes are separated by a distance larger than r_g, a "Josephson string" is formed, whose energy is proportional to its length[16].

When the anisotropy is not too large, the Josephson coupling among adjacent pancakes, which are loosely belonging to the same "flux-line", dominates over the electromagnetic interaction, and the later can be neglected. The ratio of the coefficients of the quadratic terms in the effective electromagnetic interaction (as mentioned above) and the Josephson interaction goes roughly like $\gamma^2(d/\lambda)^2$ (where $d/\lambda \sim 1/120$ for BSCCO at $T = 0$ and even smaller at higher temperatures). Thus for anisotropy $\gamma = 50$ we get a factor of 0.25 or less (a somewhat more precise estimate[17] gives a ratio of about 0.1). Thus the magnetic interaction is small compared to the Josephson interaction for anisotropies in the range of $\gamma = 50 - 100$. For samples with $\gamma = 200$ these interactions are already comparable. For large values of R the magnetic interaction increases logarithmically and the Josephson interaction increases

linearly so the electromagnetic interaction is always negligible. The key to the estimate given above is to consider not just two pancake vortices but a whole line with one displaced pancake. This argument is valid if the deviations of the vortices from straight lines are not too large. On the other hand, the electromagnetic interaction starts to be important for anisotropies which are significantly larger than λ/d which for BSCCO is about 120.

It is the aim of this paper to include both the electromagnetic interaction and the Josephson interaction among pancakes and to see what is the combined effect on the phase diagram of the melting transition and the energy jump across the transition. The electromagnetic interaction will be included fully in the sense that we will not make the approximation that the pancake stacks are nearly straight and hence the electromagnetic coupling will not be replaced by an in-plane effective coupling. Numerically, much of the past work on BSCCO has been confined to the X-Y model[19,20,21,22,23,24] and Bose model[17,25], both of them treat the electromagnetic coupling imprecisely by including it as an effective in-plane interaction. Recently in several papers using the Langevin simulation method[26,27,28], the electromagnetic coupling has been fully taken into account. Unfortunately, these papers completely neglect the Josephson coupling which can hardly be justified. Also some of these papers work with a small system size like 5 to 10 planes along the z-direction, and some do not even use periodic boundary conditions in the z-direction. In this paper we carry out Monte Carlo simulations of a BSCCO system consisting of $20-36$ planes and periodic boundary conditions are used in all directions, including the z direction. Thus a pancake would interact with an infinite number of pancakes through the images under the periodic boundary conditions. For this an efficient way to sum over the interaction is required. We derive a formula for summing over the logarithmic interaction in Appendix B.

II. THE MODEL

The starting point is the Lawrence-Doniach[29] Gibbs free-energy functional,

$$\begin{aligned}\mathcal{G}[\psi_n, \mathbf{a}] \;=\; & \int d^2\mathbf{R} \sum_n \alpha|\psi_n|^2 + \frac{\beta}{2}|\psi_n|^4 + \frac{\hbar^2}{2m}\left|\left(\frac{\nabla^{(2)}}{i} + \frac{2\pi}{\phi_0}\mathbf{a}^{(2)}\right)\psi_n\right|^2 \\ & + \frac{\hbar^2}{2Md^2}\left|\psi_{n+1}\exp\left(\frac{2\pi i}{\phi_0}\int_{n\,d}^{(n+1)d} dz\, a_z\right) - \psi_n\right|^2 \\ & + \int d^2\mathbf{R}dz\left(\frac{b^2}{8\pi} - \frac{\mathbf{b}\cdot\mathbf{H}}{4\pi}\right), \end{aligned} \tag{2.1}$$

where ψ_n represents the superconducting order parameter in the n^{th} CuO_2 layer, $\mathbf{a}^{(2)}$ is the vector potential in the plane, and d is the thickness of the insulating layers. $\mathbf{b}$ is the local magnetic field and $\mathbf{H}$ the externally applied field. The usual 3D integration of the GL theory has been replaced by a summation over all the superconducting layers along with a 2D integration over the superconducting planes. We set $\psi_n = |\psi_n|\exp(i\phi_n)$ and, working in the London approximation, we drop the term $\alpha|\psi_n|^2 + \beta|\psi_n|^4/2$ because it gives only a constant contribution. Then we get

$$\begin{aligned}\mathcal{G} = \int d^2\mathbf{R}\,\frac{\varepsilon_0 d}{2\pi}\Bigg(\int dz\,\sum_n \delta_2(z - n\,d)\left(\frac{\nabla^{(2)}\phi_n}{i} + \frac{2\pi}{\phi_0}\mathbf{a}^{(2)}\right)^2 \\ + \frac{2m}{Md^2}\sum_n\left[1 - \cos\left(\phi_{(n+1)} - \phi_n + \frac{2\pi}{\phi_0}\int_{nd}^{(n+1)d} dz\, a_z\right)\right]\Bigg) \\ + \int d^2\mathbf{R}dz\left(\frac{b^2}{8\pi} - \frac{\mathbf{b}\cdot\mathbf{H}}{4\pi}\right), \end{aligned} \tag{2.2}$$

where

$$\varepsilon_0 = 2\pi\frac{\hbar^2|\psi_n|^2}{2m} = \frac{\phi_0^2}{(4\pi\lambda)^2}. \tag{2.3}$$

Minimization with respect to a_x (i.e. $\frac{\delta\mathcal{G}}{\delta a_x} = 0$) and a_y (i.e. $\frac{\delta\mathcal{G}}{\delta a_y} = 0$) gives

$$\lambda^2\triangle\mathbf{a}^{(2)} = d\sum_n \delta_2(z - n\,d)\left[\mathbf{a}^{(2)} + \frac{\phi_0}{2\pi}\nabla^{(2)}\phi_n\right], \tag{2.4}$$

where $\triangle$ stands for the 3-dimensional Laplacian. Minimization with respect to a_z gives

$$\frac{\varepsilon_0 d}{2\pi}\frac{2m}{Md^2}\frac{2\pi}{\phi_0}\sin(\Phi_{(n,n+1)}) + \frac{1}{4\pi}\left(\nabla\times(\nabla\times\mathbf{a})\right)_z = 0, \tag{2.5}$$

where

$$\Phi_{n+1,n} = \phi_{n+1} - \phi_n + \frac{2\pi}{\phi_0}\int_{nd}^{(n+1)d} dz\; a_z \tag{2.6}$$

is the gauge invariant phase difference between the layers n and $n+1$. Eq. (2.5) implies

$$\Delta a_z = \frac{4\pi}{c} j_J \sin(\Phi_{n,n+1}). \tag{2.7}$$

where

$$j_J = \frac{c\phi_0}{8\pi^2\lambda^2\gamma^2 d} \tag{2.8}$$

is the Josephson-coupling current density between layers. Minimization with respect to ϕ_n gives

$$\Delta^{(2)}\phi_n + \frac{2\pi}{\phi_0}\nabla^{(2)} \cdot \mathbf{a}^{(2)} = \frac{1}{\gamma^2 d^2}\left[\sin(\Phi_{n,n-1}) - \sin(\Phi_{n+1,n})\right]. \tag{2.9}$$

Eqs. (2.4), (2.7) and (2.9) are to be solved with the appropriate boundary conditions and the solution must be substituted back into Eq. (2.2) to obtain the Gibbs free-energy, and thus the strength of the interaction among pancake solutions. We also see that in the limit of infinite anisotropy the right-hand-side of equations (2.7) and (2.9) tend to zero. An isolated pancake residing in plane n is a singular solution of the equation for the phase of the wave function which satisfies

$$\nabla^{(2)}\phi_n(\mathbf{R}) = -\frac{\mathbf{n}\times(\mathbf{R}-\mathbf{R}_n)}{(\mathbf{R}-\mathbf{R}_n)^2}, \tag{2.10}$$

where $\mathbf{R}$ is a two dimensional vector in the plane and $\mathbf{R}_n$ denotes the center of the pancake. By $\mathbf{n}$ we denote a unit vector in the z-direction. Thus as one fully encircles the pancake the phase ϕ_n changes by 2π, and is singular at the center of the pancake. In the case when the Josephson coupling is totally neglected, i.e. for $\gamma \to \infty$, the full solution of Eqs. (2.4), (2.7) and (2.9) can be found and from it one can easily obtain the magnetic-field in real space[12]. It is not a trivial matter to switch from the variables ϕ_n and $\mathbf{a}$ to pancake variables and express the free energy in terms of the latter. This transformation can only be implemented approximately. In the following we first summarize the known results for the Josephson interaction and the electromagnetic interaction and then proceed to combine them together into a single algorithm. Most papers consider only one type of interaction, Josephson or electromagnetic in the limit that one dominates over the other.

A. Josephson Coupling

We keep the same Josephson coupling as in Ref. 25. This coupling is strongly dependent on the anisotropy parameter γ. Consider two adjacent pancakes, belonging to the same FL,

residing in the m and $m+1$ planes respectively, such that their centers are displaced and not located on top of each other. Assume that the pancake on the $m+2$'th plane is located on top of the $m+1$-plane pancake, and the pancake residing in the $m-1$ plane is at the same position as the m-plane pancake. Thus $\phi_{m+1} \neq \phi_m$ but $\phi_{m+2} = \phi_{m+1}$ and $\phi_{m-1} = \phi_m$. This assumption is made in order to trancate the infinite set of couples equations[2], and in real situations may constitue an approximation. Denoting $\Phi_{m+1,m} = \phi_{m+1} - \phi_m$ simply by Φ we see that writing down Eq. (2.9) for the m and $m+1$ planes respectively and subtracting one equation from the other, one obtains

$$\mathbf{\Delta}^{(2)}\Phi = \frac{2}{r_g^2}\sin(\Phi), \tag{2.11}$$

where $r_g = \gamma d$ is the relevant screening length of the problem. Note that the screening term due to the vector potential has been neglected since it is negligible on length scales $R \sim r_g \ll \gamma\lambda$. Equation (2.11) is the famous Sine Gordon Equation. Once its solution is obtained, it needs to be substituted in the Lawrence-Doniach Gibbs free-energy. This results in a contribution of the form[30]

$$\mathcal{G}_J = \frac{d\varepsilon_0}{\pi r_g^2}\int d^2\mathbf{R}'[1-\cos(\Phi(\mathbf{R}')). \tag{2.12}$$

If we denote the separation between the two pancakes by R one can show that for $R \ll R' \ll r_g$ the solution of Eq. (2.11) is given simply by

$$\Phi(\mathbf{R}') = R\sin(\theta')/R', \tag{2.13}$$

since the right-hand-side can be neglected in this region. Here θ' is the azimuthal angle in the plane. For $R' \gg r_g$ the $\sin(\Phi)$ can be replaced by Φ and we see that the solution decays exponentially with a screening length r_g. Thus substituting Eq. (2.13) into Eq. (2.12), expanding the cosine to quadratic order and cutting off the integration at a large distance $R' = r_g$ and small distance $R' = R$ the interaction energy becomes

$$\mathcal{G}_J(R) = \frac{d\varepsilon_0}{2}\ln\left(\frac{r_g}{R}\right)\left(\frac{R}{r_g}\right)^2, \tag{2.14}$$

so we see that it is approximately proportional to R^2. On the other hand when the separation between the centers of the two pancakes becomes larger than r_g then a Josephson string is formed between the m'th and the $m+1$'th planes in a direction parallel to the planes. The energy of the Josephson string is proportional to its length which is equal to R, the pancakes'

separation. The calculation of this energy is rather involved and discussed by Clem, Coffey and Hao[16]. The final result is

$$\mathcal{G}_J(R) = d\varepsilon_0 \left(1.12 + \ln\left(\frac{\lambda}{d}\right)\right)\frac{R}{r_g}. \tag{2.15}$$

The question now arises how to match these two interaction potentials valid for $R \ll r_g$ and $R \gg r_g$, one behaving quadratically in R and one linearly in R. One such extrapolation was given by Ryu, Doniach, Deutscher and Kapitulnik (RDDK)[17], who achieved a matching by keeping the coefficient of the linear term in R as given in Eq. (2.15) in both regions, choosing the matching point to be at $R = 2r_g$, and subtracting a constant so that the two expressions would vanish at the matching point. Keeping the same constant in both expressions assures that the first derivative is continuous at the matching point. RDDK also replaced the constant 1.12 by 1. There are ways to improve the extrapolation[42] but they do not change significantly the results of the simulations performed using the RDDK formula. Unfortunately there was a mistake by a factor of $\pi/2$ in the RDDK formula that we corrected below that has the effect of renormalizing the anisotropy parameter by about $\sqrt{\pi/2} \approx 1.25$ since the major contribution to the simulations come from the region $R < 2r_g$. To summarize, the London free-energy for inter-layer (IL) Josephson coupling is given approximately by:

$$\Im_{IL}(\mathbf{R}_{i,m}, \mathbf{R}_{i,m+1}) = \frac{d{\phi_0}^2}{16\pi^2\lambda^2}\left(1 + \ln\left(\frac{\lambda}{d}\right)\right)\left[\frac{(|\mathbf{R}_{i,m} - \mathbf{R}_{i,m+1}|)^2}{4{r_g}^2} - 1\right], \tag{2.16}$$

for $|\mathbf{R}_{i,m} - \mathbf{R}_{i,m+1}| < 2r_g$, and

$$\Im_{IL}(\mathbf{R}_{i,m}, \mathbf{R}_{i,m+1}) = \frac{d{\phi_0}^2}{16\pi^2\lambda^2}\left(1 + \ln\left(\frac{\lambda}{d}\right)\right)\left[\frac{|\mathbf{R}_{i,m} - \mathbf{R}_{i,m+1}|}{r_g} - 2\right], \tag{2.17}$$

for $|\mathbf{R}_{i,m} - \mathbf{R}_{i,m+1}| > 2r_g$. Here the position of a pancake is specified in terms of cylindrical coordinates. Thus the position of the i'th pancake in the m'th plane is given by $(\mathbf{R}_{i,m},\ md)$, where $\mathbf{R}_{i,m}$ is a two dimensional vector in the ab plane. The index i labels the FL that the pancake is a part of. We have considered only pancakes belonging to the same FL. This is because for large separations by definition the Josephson string is formed among pancakes belonging to the same FL. We do check for the energy of all nearest neighboring pairs when deciding how to connect pancakes and we allow the process of flux "cutting" and switching. In the case that pancakes belonging to different FL's approach each other to a distance much smaller than r_g, than there will be an interaction of the form of Eq. (2.14), however

this occurrence is rather rare for magnetic fields of the strength considered here and hence neglected by RDDK and also in this work.

When using Eqs.(2.16) and (2.17) it is necessary to specify the temperature dependence of λ. Different choices for this dependence are found in the literature. In this work we used the same choice as in Refs.[2,17,34], motivated by Ginzburg-Landau (GL):

$$\frac{\lambda^2(0)}{\lambda^2(T)} = 1 - T/T_c. \tag{2.18}$$

Some authors[18,37] use a dependence of the form

$$\frac{\lambda^2(0)}{\lambda^2(T)} = 1 - (T/T_c)^2. \tag{2.19}$$

Recent experiments[35] show that the temperature dependence of the london penetration depth is not universal and depend on the amount of doping and the sample history. In Fig. (1) we show the temperature dependence of the three samples investigated in Ref.[35]. Also shown on the figure is the two fluid dependence[1] $\lambda^2(0)/\lambda^2(T) = 1 - (T/T_c)^4$ which normaly applies in the opposite limit of very small GL ratio $\kappa = \lambda(0)/\xi(0)$, unlike high-Tc materials. Displayed also is the weak coupling, clean limit BCS curve. Both curves are lying above the experimental data. We added to the original figure the two behaviors given in Eqs. (2.18) and (2.19) to show that the experimental data actually falls between theses two curves, so they give reasonable lower and upper bounds to the experimental results. In the result section we discuss how this choice of temperature dependence affects the comparison of the simulation results with experiments.

B. Electromagnetic Coupling

This coupling can be obtained from the Lawrence-Doniach model discussed at the beginning of this section by putting $\gamma = \infty$, which eliminates the Josephson coupling altogether. Extensive calculations can be found in the literature[2,3,12]. For the in-plane interaction between two pancakes one finds,

$$\mathbf{U}(R_{ij}, 0) = 2d\varepsilon_0 \left(\left(1 - \frac{d}{2\lambda} \right) \ln \frac{C}{R_{ij}} + \frac{d}{2\lambda} E_1 \right) \ , \tag{2.20}$$

where $R_{ij} = |\mathbf{R}_{i,m} - \mathbf{R}_{j,m}|$ is the radial distance in cylindrical coordinates and "m" denotes the index of the plane.

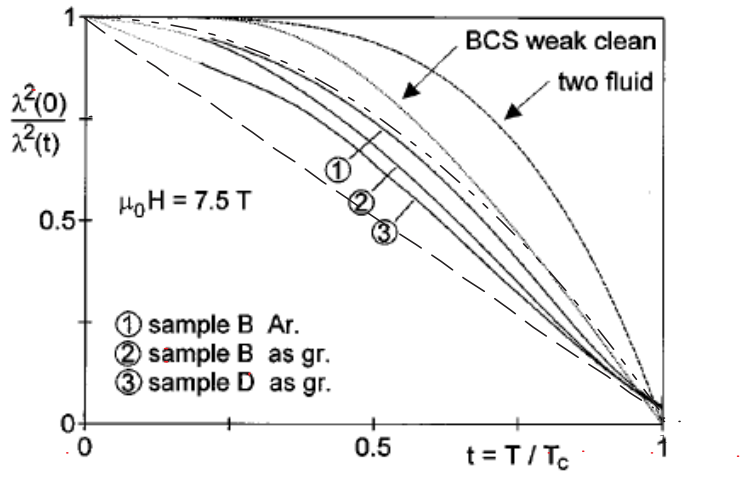

FIG. 1: Temperature dependence of the normalized penetration depth for 3 experimental samples as given in Ref. 35. For comparison the two-fluid and BCS result for clean superconductors in the weak coupling limit are shown. We also added the linear and quadratic behavior as given in Eqs. (2.18) and (2.19) in the text, represented by dashed and dot-dashed lines respectively.

The interaction between two pancakes situated at different planes ($\mathbf{R}_{i,m},\ md$) and ($\mathbf{R}_{j,n},\ nd$) is given by,

$$\mathbf{U}(R_{ij}, z) = -\frac{d^2\varepsilon_0}{\lambda}\left(\exp(-|z|/\lambda)\ln\frac{C}{R_{ij}} - E_2\right)\ , \tag{2.21}$$

where $R_{ij} = |\mathbf{R}_{i,m} - \mathbf{R}_{j,n}|$, and $z = (m-n)d$.

In the above equations we defined

$$E_1 = \int_{R_{ij}}^{\infty} d\rho \exp(-\rho/\lambda)/\rho, \tag{2.22}$$

$$E_2 = \int_{R_{ij}}^{\infty} d\rho \exp(-\sqrt{z^2+\rho^2}/\lambda)/\rho, \tag{2.23}$$

C is a constant of the order of the system's size that cancels out upon taking energy differences.

III. NOTES ON THE SIMULATIONS

We work with M rhombically shaped cells stacked on top of each other in z direction. All of these cells have periodic boundary conditions in x and y directions. Each one of

these rhombic units cells also repeats itself every M^{th} plane due to the periodic boundary condition in z direction as well. Thus we have periodic boundary conditions in all directions. There are a total of N pancakes in each of the M cells. We work with two system sizes to safeguard against any possibile finite size effects. While working with $N = 36$ we chose $M = 25$ in most cases, except for $B = 100$ G and $\gamma \leq 150$, where the number of planes was increased from 25 to 36. For low fields and anisotropies the entanglement length along the c axis becomes large, and hence in order to observe a sharp transition a larger system size in the z-direction is needed. Similarly, for 64 pancakes in each plane, we usually work with a total of 20, 25 or 36 planes depending on the values of parameter B and γ. In all the cases considered in this paper we always had a total of at least 900 beads ($N = 36$, $M = 25$) and a maximum of 2304 beads ($N = 64$, $M = 36$). A FL consists of one pancake from each and every plane. Pancakes belonging to a given FL were tracked with pointers and linked lists[31].

Pancakes were moved by either Metropolis algorithm[31] or its advance form, multilevel Monte Carlo (MMC)[32]. Which method to employ in a particular case usually depends upon the anisotropy and the magnetic field, as described below.

For most anisotropies and magnetic fields, the MMC technique was used. In MMC we update several pancakes spread over many planes at once. Thus for the lower anisotropies $\gamma = 125$ and 150, and $B = 100$ G, a total of 15 to 20 beads spread over 5 planes were used to update the system. For other anisotropies and fields ($\gamma \geq 250$ and $B \leq 900$ G) it suffices to use just 3 planes in the MMC technique.

For different parameter ranges, one needs to use different methods of updating the FL's. For example, one can not use MMC method for $\gamma = \infty$ since there is no natural choice to generate paths sampled with a free Gaussian distribution. Even at higher values of γ, such as 500, the MMC method using 5 planes would be slow and inefficient. Thus for $\gamma \geq 375$ and $B \geq 300$, we move only one pancake at a time using the Metropolis algorithm. Flux cutting was implemented by using a different kind of move to allow for the large wiggling of the FL's (and thus to avoid bias towards straighter FL configurations). In this move the two ends of neighboring lines were switched by considering only the relevant Josephson interactions without attempting to displace any of the pancakes involved.

Just like the case with high anisotropies discussed above, in the MMC implementation also we allowed for large wiggling of FL's along the z-direction by introducing the process of flux cutting. Starting from a few neighboring lines, we cut chunks of FL's spreading over a

number of planes. New paths between the starting and ending positions of the FL's thus cut were made using a random walk through the space of permutations[13] and the subsequent use of the bisection method[32].

Of course there are ranges of parameters where more than one method of update can be employed (e.g. Metropolis method, MMC with 3 planes or MMC with 5 planes.). In these cases of overlap, relevant methods were found to lead to the same result, as they should. Further details on the simulation technique are supplied in Ref. 25.

The logarithmic part of the in-plane and out of plane electromagnetic interaction (see Eqs. (2.20) and (2.21)) was handled by analytically summing over the interaction as shown in the Appendix B. The integrals E_1 and E_2 were evaluated numerically taking into account the periodic boundary conditions in all directions. This is accomplished by considering images of pancakes in all directions.

In the simulations as T is raised it is B that is kept fixed, not H, as done in experiments. This causes the phase transition to be less sharp, especially at low fields (where the phase boundary is flatter), as is evident from Fig. 2. The figure shows both the $H-T$ and $B-T$ phase diagrams schematically. In the $B-T$ phase diagram there is a region where both the vortex-solid and vortex-liquid phases coexist. The paths corresponding to increasing temperature at constant B (MC) and constant H (experiment) are shown.

The broadening of the phase transition can be avoided by using 'isobaric" Monte Carlo simulations[13], but this was not done in the present work.

We measured the following physical quantities. For details the reader is referred to our earlier work[25].

A. Energy

An expression for energy can be obtained from

$$E = kT^2 \frac{\partial}{\partial T} \ln(\Xi(\Lambda, \beta, N)). \tag{3.1}$$

Due to the internal temperature dependence of λ on T, one gets a very complicated expression for energy (not written down here). However, a simplified expression for energy can be obtained under the assumption that $a_0 < \lambda$, since in this case it is justified to ignore the internal temperature dependence of λ on T while taking derivatives with respect to the

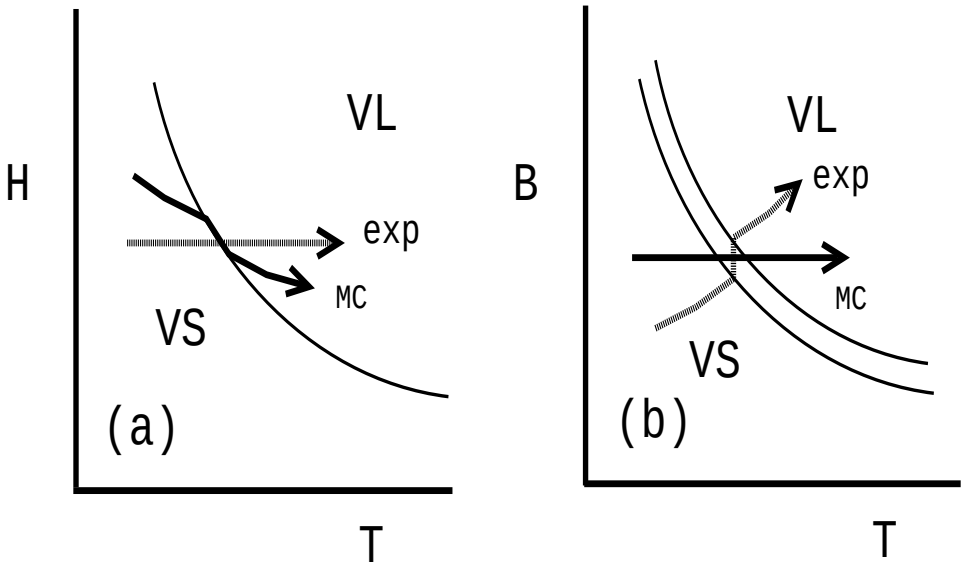

FIG. 2: Schematic phase diagram showing the vortex-solid (VS) and votex-liquid (VL) phases in the $H-T$ and $B-T$ planes. The path the system traces as the temperature is raised at fixed B (MC) or fixed H (exp) are indicated

temperature[13]. The energy expression obtained for the case when $a_0 < \lambda$ is given in Ref. 25. This expression, however, was seen to work well even for the cases where $a_0 \sim \lambda$ and the difference between the simplified and the exact energy calculations was found to be insignificant for all cases except for very low values of B such as $40 - 80$ G (we used these values for only $\gamma = \infty$). We have used the simplified expression for the energy in all cases. It would not affect the melting transition in anyway. The only change will be that the energies obtained will be off by a few percents for the case when the magnetic field is very small.

B. Translational structure factor

The translational structure factor $S(\mathbf{Q}_1)$ is defined as,

$$S(\mathbf{Q}_1) = \frac{1}{MN}\left\langle \sum_{ij,m} e^{(i\mathbf{Q}_1.(\mathbf{R}_{i,m}-\mathbf{R}_{j,m}))} \right\rangle, \tag{3.2}$$

where $\langle ... \rangle$ stands for the MC average, and $\mathbf{Q}_1$ stands for a reciprocal lattice vector corresponding to the first Bragg peak and is given by

$$\mathbf{Q}_1 = \frac{2\pi}{a_0 \sin^2\theta}(\mathbf{e}_1 - \mathbf{e}_2 \cos\theta), \tag{3.3}$$

where $\theta = \pi/3$, a_0 is the nearest neighbor distance and $\mathbf{e}_{1,2}$ are the unit vectors along the hexagonal unit cell such that

$$\mathbf{e}_1 \cdot \mathbf{e}_2 = \cos\theta. \tag{3.4}$$

C. Line entanglement

As we allow permutations of FL's, we can define a number N_e/N as that fraction of the total number of FL's which belong to loops that are bigger than the size of a "simple" loop. A simple loop is defined as a set of M beads connected end to end, M being the total number of planes. Loops of size $2M$, $3M$... start proliferating at and above the transition temperature and in the corresponding 2D boson system this proliferation is related to the onset of the superfluidity.

Some of the other important parameters were taken as follows: $\lambda_0 = 1700$ Å, $d = 15$ Å and $T_c = 90$ K.

IV. RESULTS

A. Josephson and electromagnetic coupling

In this section we discuss the results when Josephson as well as electromagnetic couplings are included in the expression for the free-energy functional. Three different quantities, the translational structure factor at the first Bragg peak $S(\mathbf{Q}_1)$, the energy E and the line entanglement N_e/N were monitored. Simulations were done for four different anisotropy parameters $\gamma = 125, 250, 375$ and 500. In addition we carried out simulations for two different temperature dependence of the penetration depth. The results for the first temperature dependence of λ, namely $\lambda^2(0)/\lambda^2(T) = 1 - T/T_c$, are shown in Figs. (3)-(6). The results for the second dependence of λ, i.e. $\lambda^2(0)/\lambda^2(T) = 1 - (T/T_c)^2$ will be discussed later, in the context of the phase diagram.

To check against possible finite size effects we worked with two different system sizes, namely 36 and 64 FL's, as discussed in the previous section. The structure factor at the first Bragg peak, for the two different sizes is shown in panels (a) and (c) of Figs. 3-6. It is clear that the transition temperature is unaffected by the choice of the system size. Similar

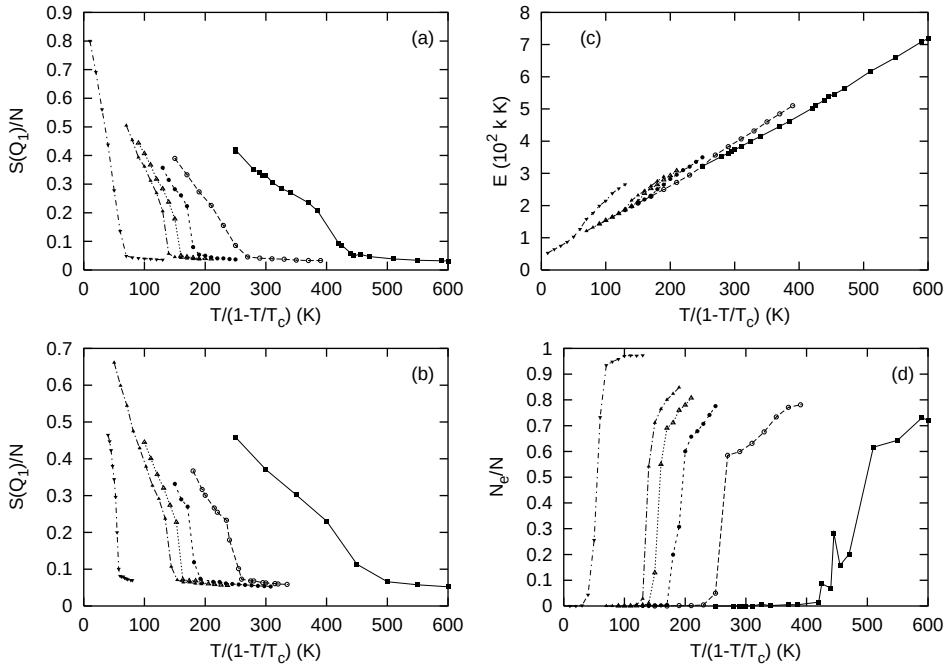

FIG. 3: $\gamma = 125$. For various fields $B = 100$ G (filled squares), 300 G (open circles), 500 G (filled circles), 700 G (open triangles), 900 G (filled triangles) and 5000 G (lower triangles), the following quantities are shown: (a) the translational structure factor at the first Bragg peak for $N = 64$ FL's (b) the translational structure factor at the first Bragg peak for $N = 36$ FL's (c) Energy for $N = 64$ FL's (energy is given up to an additive constant, which is not important.) (d) Line entanglement for $N = 64$ FL's.

agreement was seen in plots of energy vs. temperature and the graphs of entanglement vs. temperature. These later comparisions are not displayed.

A first-order transition (FOT) is seen for all anisotropies, which is in agreement with numerous experimental[4,5,7,8] as well as numerical[13,17,19,21,24,25,33,34] studies on type-II superconductors. The location of the FOT is inferred from a sharp decay in $S(\mathbf{Q}_1)$ and a sharp rise in the line entanglement and a discontinuous jump in energy E. Except for the case with $\gamma = 125$ and $B = 100$ G, the transition is sharp and can be easily located. In all the cases, we see a discontinuous jump in E. The size of the jump can be determined in the following way. Take two sets of points on E vs. $T_r = T/(1 - T/T_c)$ graph, one in the vortex solid phase and the other in the vortex liquid phase. This can be done by using $S(\mathbf{Q}_1)$ or N_e/N vs. T_r graphs. We fit a straight line to the first set of points and another straight line

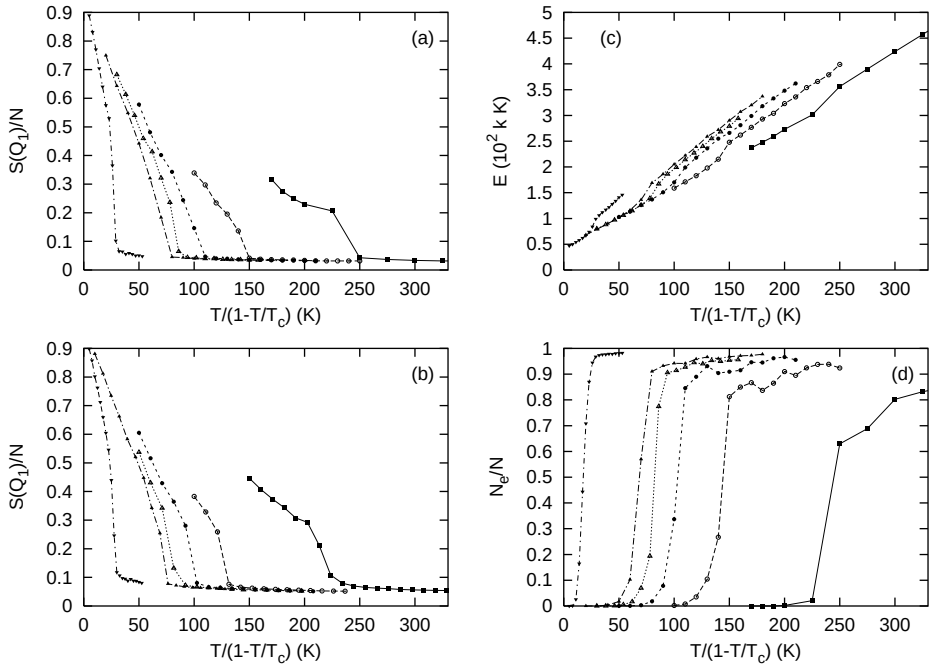

FIG. 4: $\gamma = 250$. The same quantities are shown as in Fig. 3 but $\gamma = 250$ here.

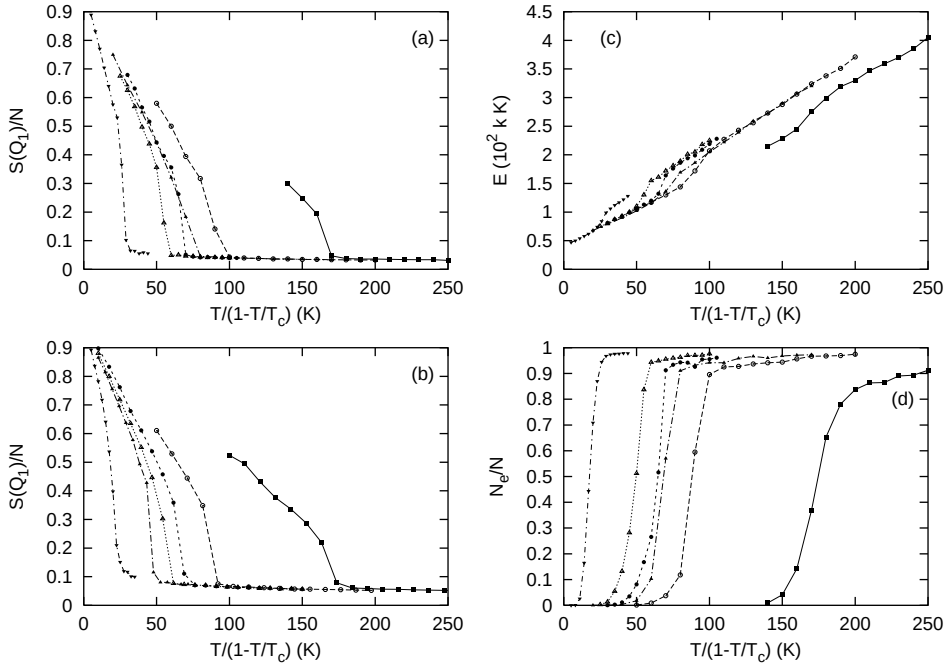

FIG. 5: $\gamma = 375$. The same quantities are shown as in Fig. 3 but $\gamma = 375$ here.

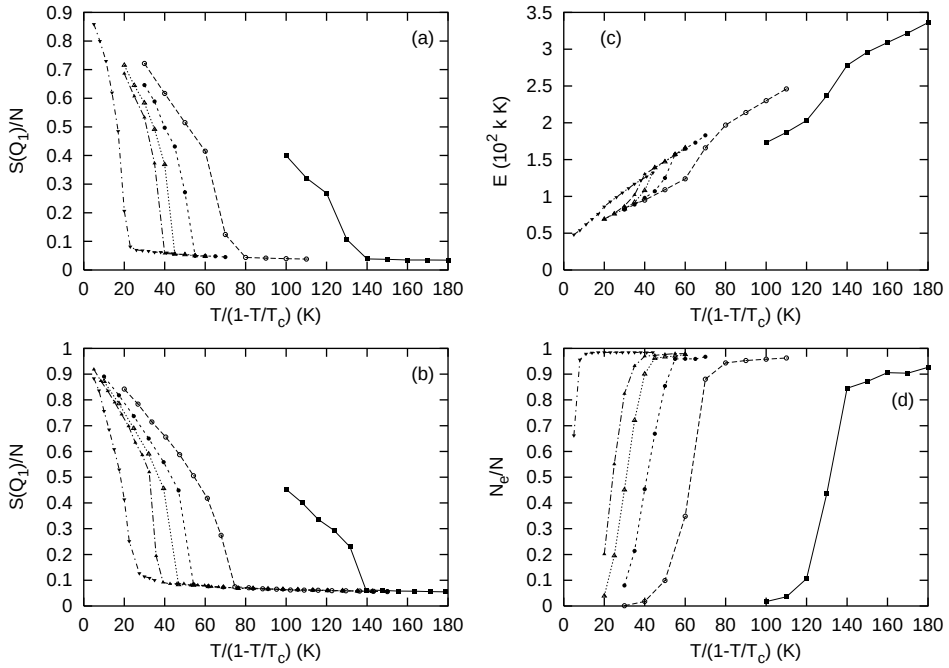

FIG. 6: $\gamma = 500$. The same quantities are shown as in Fig. 3 but $\gamma = 500$ here.

to the other set of points. The two lines are extended up to the transition temperature and the jump in E is read off.

It is clear from the E vs. T_r graphs that for a given anisotropy one gets lower jumps in E at higher magnetic fields. This effect is more pronounced for higher anisotropies.

B. Only electromagnetic coupling

Many simulation studies completely neglect the Josephson coupling[26,38] and work only with the electromagnetic coupling. In this section we discuss the results obtained with neglecting the Josephson interaction ($\gamma = \infty$). The results are shown in Fig. 7. The results can be compared with a recent simulation study of the same system using substrate model[37,38]. The phase boundary obtained by Dodgson *et al.* falls almost on top of the phase boundary obtained in this paper. Another important feature of this study is the increasing energy jumps toward lower magnetic fields as well as almost diminishing jumps in E toward very high magnetic fields ($B > 900$ G). The entropy jump calculated using the formula $\Delta s = \Delta E/T$ shows an increasing trend towards higher temperature (not shown here) again in agreement with the references cited above.

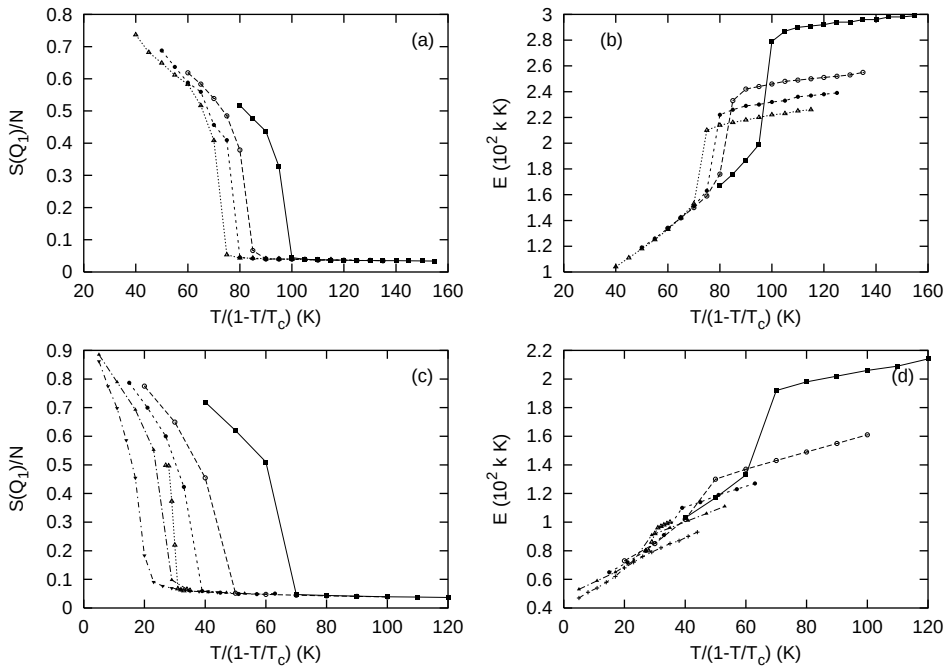

FIG. 7: $\gamma = \infty$ (no Josephson coupling). (a) the translational structure factor at the first Bragg peak for $B = 40$ G (filled squares), 60 G (open circles), 70 G (filled circles), 80 G (open triangles). (b) Energy for the same fields as in (a) (c) the translational structure factor at the first Bragg peak for $B = 100$ G (filled squares), 300 G (open circles), 500 G (filled circles), 700 G (open triangles), 900 G (filled triangles) and 5000 G (downward triangles). (d) Energy for the same fields as in (c).

Also, for the very high magnetic fields, the transition takes place at $T_{2D} = 16$ K, independent of the magnetic field. This result is in agreement with many theoretical studies[2,18]. In this regime of fields each set of pancakes in a plane melts irrespective of the other planes and shows a characteristic 2D melting transition at $T_{2D} \approx 16 - 19$ K. This kind of 2D melting is expected at high fields as the in-plane pancakes get closer to each other and hence the in-plane interaction keeps getting stronger compared to out of plane interaction and the different layers start to melt independent of each other[26].

Comparing results with the previous section, it is clear that the Josephson interaction, present at finite anisotropy, has the effect of reducing the energy jumps compared to the case when only the electromagnetic coupling is included.

C. Phase diagram

Based on the results from the previous two sections, we obtain a phase diagram for BSCCO which is shown in Fig. 8. The diagram shows the melting curves for various anisotropies, including the case when there is no Josephson coupling. On the same diagram we also show two experimental lines, one for the melting transition[7,39] and the other for the irreversibility line[40]. The experimental irreversibility line falls very close to the simulated $\gamma = 250$ phase boundary. The actual experimental melting curve does not seem to fall on any of the melting lines obtained from the simulations. The experimental melting line bends downward toward lower temperatures and this feature could not be seen here. This may the result of point defects present even in pristine samples, an effect reported in recent simulations[22,23].

In Fig. 9 we show the phase diagram obtained by assuming a different dependence of λ on temperature, namely $\lambda(T) = \lambda(0)/\sqrt{1 - T^2/T_c^2}$. For this choice the irreversibility line falls somewhat below the $\gamma = 500$ simulated phase boundary, leading to an estimate of $\gamma \approx 450$. As discussed above the temperature dependence should be somewhere in between these dependences so an estimate of $\gamma = 300 - 400$ for the experimental sample is probably reasonable.

We have found that the data for the phase boundaries can be collapsed on a single curve for the case of finite anisotropy even when using different temperature dependences of λ. When we plot the variable $B\gamma^2$ at the melting transition versus the variable $kT/(\varepsilon_0(T)d)$ all 8 curves fall on top of each other. Koshelev[21] argues that when Josephson coupling dominates over electromagnetic coupling the phase boudary is determined by a single dimensionless function of the dimensionless parameters $kT/\varepsilon_0 d$ where $\varepsilon_0(T) = \phi_0^2/(4\pi\lambda(T))^2$ and $r_g^2/a_0^2 \propto B\gamma^2$. In Fig.(10 we plot $\ln(B\gamma^2)$ versus $\ln(kT/(\varepsilon_0 d))$ and the data collapses to a straight line with slope (-2). This suggests that the transition is given by a single relation

$$\Lambda \equiv \left(\frac{kT}{\sqrt{2}\varepsilon_0 d}\right)\left(\frac{\gamma d}{a_0}\right) = \Lambda_c \tag{4.1}$$

as is known to be the case for YBCO[13]. From a simple cage model (see e.g. Ref. 36) it follows that the $\Lambda_c = c_L^2$, where c_L is the Lindemann coefficient. This means that the transition occurs when the mean square devaiation of the FL from a straight line exceeds $c_L a_0$, where a_0 is the lattice constant. Since we find that $\Lambda_c \approx 0.1$, it appears that $c_L \approx 0.3$

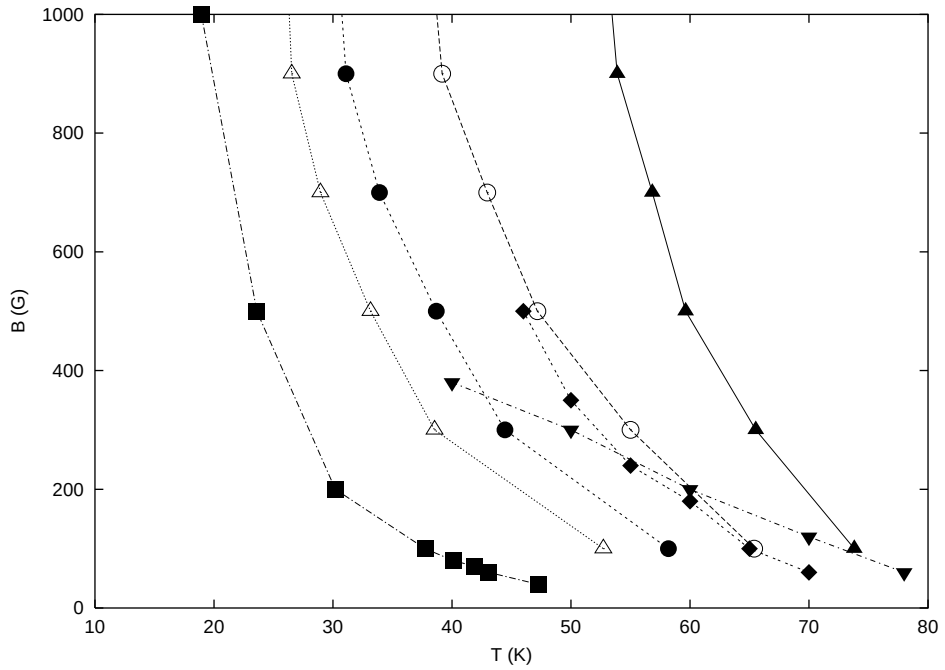

FIG. 8: Phase diagram obtained by using $\lambda(T) = \lambda(0)/\sqrt{1 - T/T_c}$: Melting transitions for various anisotropies $\gamma = 125$ (filled triangles), $\gamma = 250$ (open circles), 375 (filled circles), 500 (open triangles), ∞ (filled squares) and experimental(inverted triangles and diamonds) are shown.

(It was estimated to be 0.25 for YBCO[13]). Notice that actually the expression for Λ should be $kT/(a_0\sqrt{2\varepsilon_l\varepsilon_0})$ and we have used $\varepsilon_l = \varepsilon_0/\gamma^2$. Had we included the factor $\ln(\lambda/d)$ in ε_l we would have obtained $\Lambda_c = 0.1/\sqrt{5} \approx 0.045$ and $c_L \approx 0.2$. Thus c_L turns out to be comparable to that found for YBCO. This phase diagram shows the importance of keeping the Josephson coupling. Even if the anisotropy parameter is as large as $\gamma = 500$, it is still not appropriate to neglect the Josephson coupling entirely.

For $\gamma = \infty$ there is another scaling which collapses the data[37,38] for the two kinds of temperature dependence we considered, namely plotting B/B_λ at the melting transition vs. $kT/(\varepsilon_0 d)$, where $B_\lambda = \phi_0/\lambda^2(T)$. This is an approximate scaling of the electromagnetic interaction valid when the dependence on the small parameter d/λ can be neglected. In Fig. (11) we show the collapsed data for two different temperature dependences and also compare with the result of Dodgson *et al*[37,38].

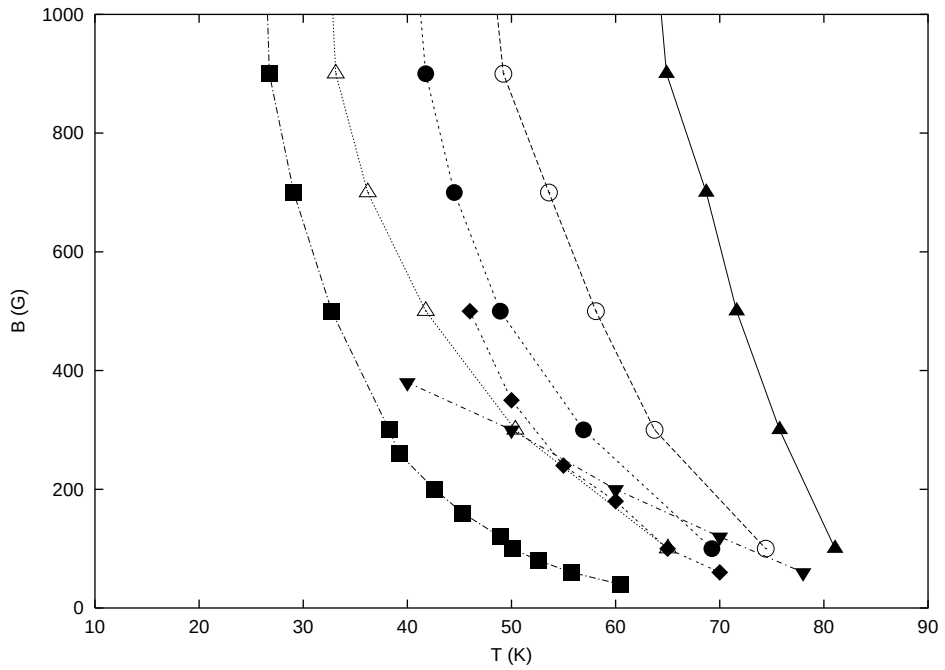

FIG. 9: Phase diagram obtained by using $\lambda(T) = \lambda(0)/\sqrt{1 - T^2/T_c^2}$: Melting transitions for various anisotropies $\gamma = 125$ (filled triangles), $\gamma = 250$ (hollow circles), 375 (filled circles), 500 (hollow triangles), ∞ (filled squares) and experimental melting transition (inverted triangles) and the experimental irreversiblity line (diamonds) are shown.

D. Comparison: local and nonlocal interactions

It is easy to show that the expression for the interaction of a single pancake with an infinite set of pancakes stacked on top of each other reduces to the modified Bessel function of second kind $K_0(R/\lambda)$ where R is the distance of the pancake from the stack of the pancakes (see Appendix A). At lower temperatures, magnetic field and anisotropy, the FL's are straight so it has been considered a good approximation to replace the nonlocal interaction between the pancakes with a local one of type mentioned above. For example we have used this model in a recent simulation[25]. In this section we compare the results obtained by replacing the nonlocal electromagnetic interaction with a local interaction of the K_0 type. The results are shown in Fig. 12, assuming the temperature dependence $\lambda^2(0)/\lambda^2(T) = 1 - t$. In Fig. 12(a) we show the phase lines for $\gamma = 125$ and 250. The phase lines for $\gamma = 125$ from the two models fall almost on top of each other. Even for $\gamma = 250$ the deviation is still small. This is reasonable, as one expects that the FL deviates less from a straight line configuration when

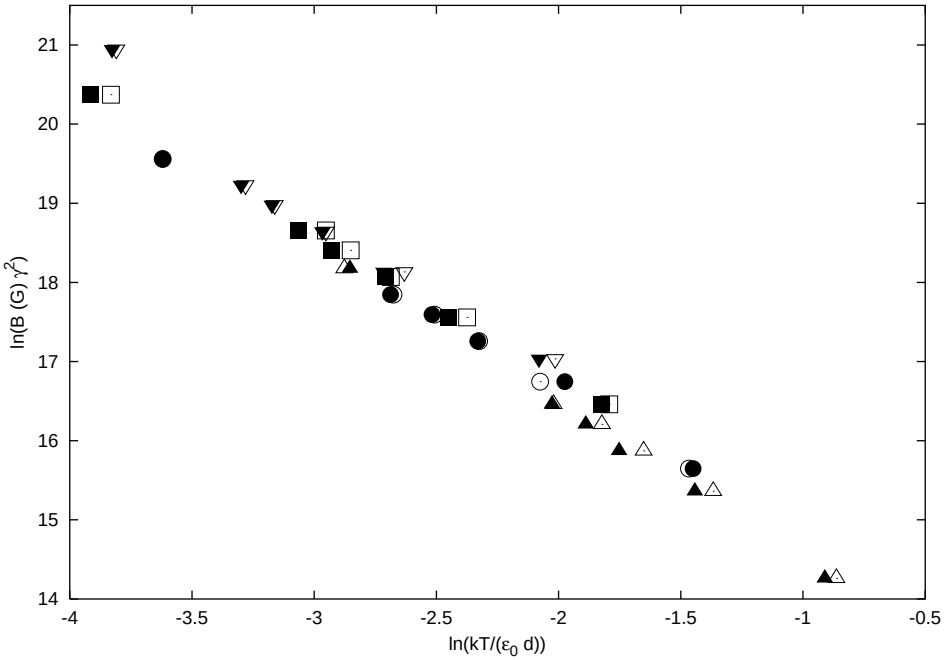

FIG. 10: Data for finite anisotropies $\gamma = 125$ (triangles),250 (circles),375 (squares) and 500 (inverted triangles) from Fig. 8 and Fig. 9 collapse onto a single curve. Filled symbols are for the $\lambda^2(T) = \lambda^2(0)/(1 - T/T_c)$ dependence while hollow symbols are for $\lambda^2(T) = \lambda^2(0)/(1 - T^2/T_c^2)$ dependence. Some spread in the data is attributed to the fact that this scaling is not valid at high values of anisotropies where Josephson coupling becomes comparable to the electromagnetic coupling.

γ is small. In Fig. 12(b-d) we compare the results obtained here with a previous paper[25] for $\gamma = 125$ and $B = 125$ G. There is a small shift in transition temperature of about 3 K. It is clear that if one shifts the $S(\mathbf{Q}_1)$ line obtained with $K_0(R/\lambda)$ interaction by around 3 K to the right, then the two curves will fall almost on top of each other.

Fig. 12(b) compares the energy jumps for the same two case as in Fig. 12(b). Except for slight shift in the transition temperature, the jumps in energy are identical. Fig. 12(c) shows the line entanglement and as expected we again see a slight shift in the position where line entanglement takes place, consistent with Fig. 12(b) and 12(c).

This justifies our claim that for the smaller anisotropies ($\gamma \approx 125$) it is a good approximation to replace the non local electromagnetic interaction with a local one of the type $K_0(R/\lambda)$.

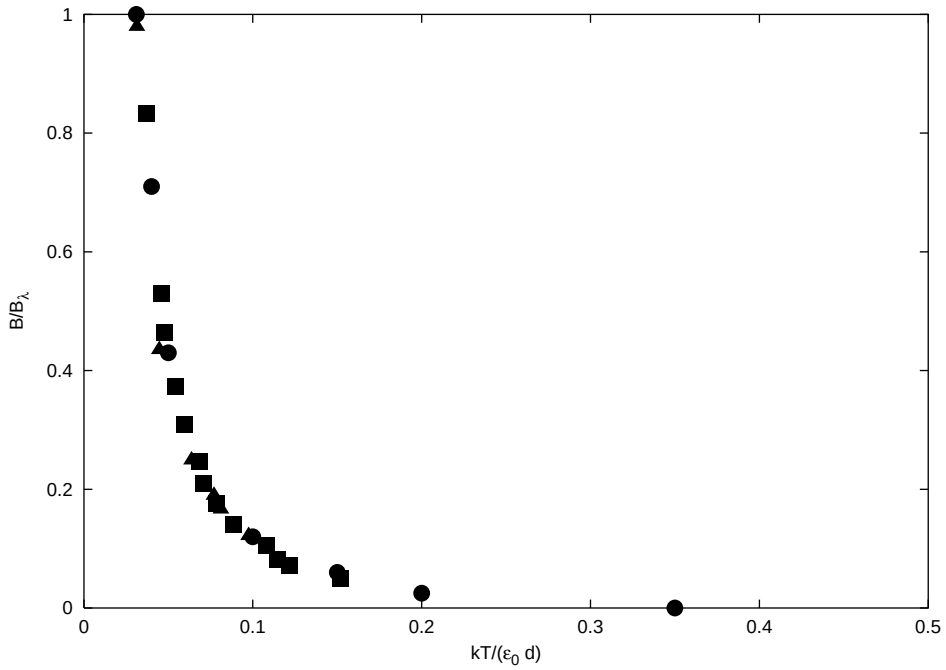

FIG. 11: Data for $\gamma = \infty$ from Fig. 8 (triangles) and Fig. 9 (squares) collapse onto a single curve. Also shown is the melting line obtained by Dodgson *et al.*[37] (circles).

V. CONCLUSIONS

In this work we introduced a model which incorporates the electromagnetic interaction and Josephson interaction among pancake vortices in the highly anisotropic BSCCO in a more systematic way than previously done. Instead of approximating the effect of the electromagnetic interaction by an in-plane repulsive interaction between pancakes that is given by a Bessel function of the second kind we treat this interaction exactly and in addition we include the Josephson coupling. Treating the electromagnetic interaction as an effective Bessel function interaction is valid only if FL's do not deviate too much from straight lines. These distortions can be quite large close to the melting transition when the flux cutting mechanism starts to proliferate. Thus in the present model interaction among pancakes is taken in a more realistic manner. There are still some approximations involved in this model but we believe that the result are more acurate than previousely obtained.

The phase boundaries for various anisotropies were obtained. It was shown that for finite anisotropy, when Josephson coupling plays a role, it tends to smoothen out energy jumps compared to the case when only the electromagnetic coupling is kept. Thus energy jumps

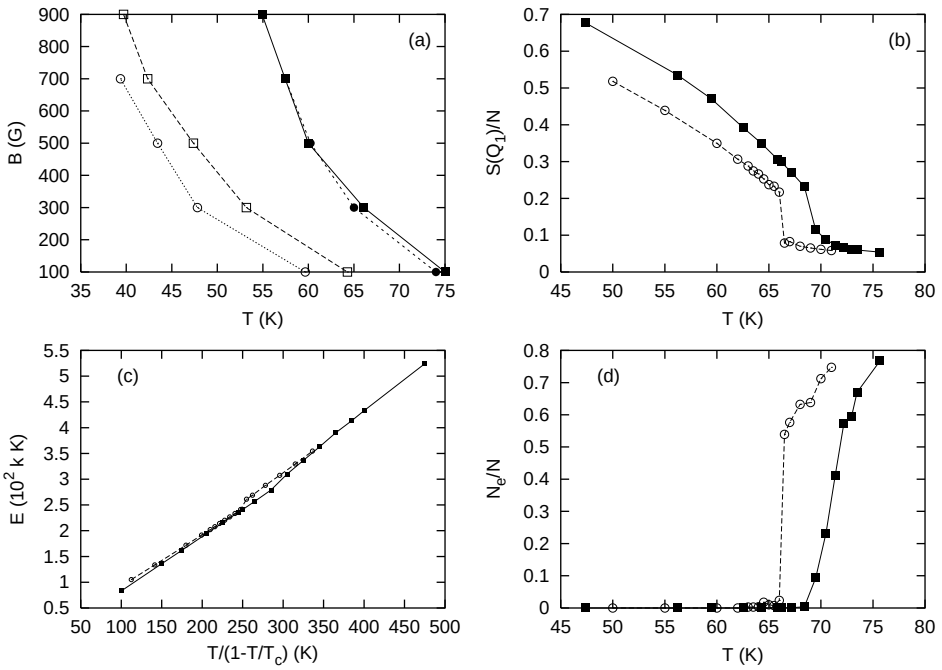

FIG. 12: Comparison between two models: (a) Phase boundaries for two different models, this paper (squares), Ref. 25 (circles) for anisotropy $\gamma = 125$ (solid squares and circles) and $\gamma = 250$ (blank squares and circles). (b) $S(\mathbf{Q}_1)$ vs. temperature for $\gamma = 150$. this paper(solid squares), Ref. 25(open circles) (c) and (d) show E and N_e/N with the same symbols and γ value as in part (b)

tend to increase with increasing anisotropy. They are also found to decrease with increasing magnetic field along the phase boundary. The phase diagram clearly shows a shift in the transition temperature as a function of the anisotropy.

For finite anisotropy up to a value of 500 we showed that the data can be collapsed to a straight line in the ln-ln plot of $B\gamma^2$ versus $kT/\varepsilon_0 d$ meaning that the transition occurs when a single variable combination of temperature, magnetic field and anisotropy becomes critical. From here we could deduce the value of the Lindemann parameter to be about 0.3. For infinite anisotropy we obtained scaling when plotting $B\lambda^2/\phi_0$ vs. $kT/\varepsilon_0 d$.

While keeping just the electromagnetic coupling we observe a typical 2D melting behavior towards high magnetic fields where the transition temperature $T_{2D} \sim 16$ K becomes independent of the magnetic field. Our results for $\gamma = \infty$ were compared with a recent simulation study using the substrate model[37,38]. The agreement between the two results is excellent.

Finally we have compared the two cases where the electromagnetic interaction is treated approximately (Ref. 25) and exactly (this paper) for a value of $\gamma = 125$. It is shown that in this case transition temperatures are very close and keeping just the in-plane interaction in the form of a modified Bessel function of the second kind is a good approximation, justifying the claim that we have made in a previous paper[25]. In that paper our main goal was to extract the effect of columnar pins on the melting transition. For larger anisotropies the deviations of the two treatments become more pronounced.

Comparing with experimental results the simulations seem to agree better with the position of the so-called irreversibility line than with the position of the true melting line. This may be due to the effect of point defects in the experimental samples. Even pristine sample contains point defects that tend to shift the phase boundary towards lower temperatures and flatten it out somewhat at the low temperature side. Point defects can also have an effect on the energy and entropy jumps across the phase boundary. If one would like to extract the value of the anisotropy of the experimental sample from the coparison with the present simulations, we would estimate it to be in the 250-450 range.

VI. ACKNOWLEDGMENTS

This work is supported by the US Department of Energy (DOE), Grant No. DE-FG02-98ER45686. YYG also thanks the Kavli Institute for Theoretical Physics (KITP) in Santa Barbara for its hospitality, where part of this paper has been finalized.

APPENDIX A: STRAIGHT FLUX-LINE APPROXIMATION

In this section we show that the interaction of a pancake with a stack of pancakes located at a distance R away from the given pancake and lined up along the z direction reduces to the modified Bessel function of the second kind, $K_0(R/\lambda)$.

Consider the interaction of a pancake situated at z=0 with a stack of pancakes. We begin with Eq. (2.20) and (2.21). The total interaction of the pancake with the FL will be given by

$$\mathbf{U}_{total}\left(\frac{R}{\lambda}\right) = 2\,d\,\varepsilon_0 \ln\frac{C}{R} + Y_1\left(\frac{R}{\lambda}\right) + Y_2\left(\frac{R}{\lambda}\right), \tag{A1}$$

where $Y_1(R/\lambda)$ and $Y_2(R/\lambda)$ are given by

$$Y_1\left(\frac{R}{\lambda}\right) = -\frac{d^2\varepsilon_0}{\lambda}\left(\sum_{m=-\infty}^{+\infty}\exp(-|m\,d|/\lambda)\right)\ln\frac{C}{R}, \tag{A2}$$

and,

$$Y_2\left(\frac{R}{\lambda}\right) = \frac{d^2\varepsilon_0}{\lambda}\left(\sum_{m=-\infty}^{+\infty}\int_R^\infty dR'\,\frac{\exp(\,-\sqrt{|m\,d|^2+R'^2}/\lambda\,)}{R'}\right). \tag{A3}$$

We have a geometric series in Eq. (A2) which can easily be summed over to give

$$Y_1\left(\frac{R}{\lambda}\right) = -\frac{d^2\varepsilon_0}{\lambda}\left(\frac{1+\exp(-d/\lambda)}{1-\exp(-d/\lambda)}\right)\ln\frac{C}{R}. \tag{A4}$$

As $\lambda/d \sim 120$ so we can approximate Eq.(A4) with

$$Y_1\left(\frac{R}{\lambda}\right) = -2\,d\,\varepsilon_0\,\ln\frac{C}{R},. \tag{A5}$$

Replacing the summation over m to an integration over z and changing the order of integration we can express $Y_2\,(R/\lambda)$ as

$$Y_2\left(\frac{R}{\lambda}\right) = \frac{d\,\varepsilon_0}{\lambda}\left(\int_R^\infty dR'\int_{-\infty}^{\infty} dz\,\frac{\exp(\,-\sqrt{z^2+R'^2}/\lambda\,)}{R'}\right). \tag{A6}$$

With a simple change of variable over z, $z = R' t$ and then again exchanging the order of integration we get

$$Y_2\left(\frac{R}{\lambda}\right) = \frac{d\,\varepsilon_0}{\lambda}\left(\int_{-\infty}^{+\infty} dt \int_R^{\infty} dR' \exp(-R'\sqrt{1+t^2}/\lambda)\right). \tag{A7}$$

Finally integrating over R' one obtains

$$Y_2\left(\frac{R}{\lambda}\right) = d\,\varepsilon_0\left(\int_{-\infty}^{\infty} dt\,\frac{\exp(-R\sqrt{1+t^2}/\lambda)}{\sqrt{1+t^2}}\right) \tag{A8}$$

$$= 2\,d\,\varepsilon_0\,K_0\left(\frac{R}{\lambda}\right). \tag{A9}$$

Combining Eq. (A1), (A5) and (A9) we get

$$\mathbf{U}_{total}\left(\frac{R}{\lambda}\right) = 2\,d\,\varepsilon_0\,K_0\left(\frac{R}{\lambda}\right). \tag{A10}$$

APPENDIX B: ENERGY SUM OVER THE IMAGES

We again consider a rhombically shaped region with side L and angle θ, unit vectors are $\mathbf{e}_1$ and $\mathbf{e}_2$ with $\mathbf{e}_1 \cdot \mathbf{e}_2 = \cos\theta$, as was done in the appendix of a previous paper.[25] The Green's function G_0 which describe the 2D coulomb interaction between one vortex and another including all its images, as is implied by the periodic boundary conditions is given by the solution to London's equation (see e.g. Ref. 1)

$$(1 - \lambda^2\nabla^2)G_0(\mathbf{R},\lambda) = 2\pi\lambda^2\delta(\mathbf{R}), \tag{B1}$$

with the parameter λ setting the scale for the range of the interaction. The solution of the above equation was derived in the appendix of Ref.25. The result was

$$G_0(\mathbf{R},\lambda) = \frac{\sin\theta}{2}\sum_{n=-\infty}^{+\infty}\frac{\cos(t_2 n - 2\pi\beta_n)\sinh(\gamma_n t_1) + \cos(t_2 n)\sinh(\gamma_n(2\pi - t_1))}{\gamma_n(\cosh(2\pi\gamma_n) - \cos(2\pi\beta_n))}, \tag{B2}$$

where

$$t_1 = \frac{2\pi R_1}{L},\ t_2 = \frac{2\pi}{L}(R_1\cos\theta + R_2),\ \beta_n = n\cos\theta,\ \gamma_n = \sin\theta\sqrt{n^2 + L^2/(2\pi\lambda)^2}. \tag{B3}$$

To get a formula for Logarithmic interaction all we have to do is to take the limit λ tends to infinity. In this limit there is only one term which diverges in the series given above namely that corresponding to $n = 0$. Separating out the term corresponding to $n = 0$ we get

$$G_0(\mathbf{R}, \lambda) = term_0 + \sin\theta \sum_{n=1}^{+\infty} \frac{\cos(t_2 n - 2\pi\beta_n)\sinh(\gamma_n t_1) + \cos(t_2 n)\sinh(\gamma_n(2\pi - t_1))}{\gamma_n(\cosh(2\pi\gamma_n) - \cos(2\pi\beta_n))}, \quad \text{(B4)}$$

where,

$$term_0 = \frac{\sin\theta}{2} \frac{\sinh(\gamma_0 t_1) + \sinh(\gamma_0(2\pi - t_1))}{\gamma_0(\cosh(2\pi\gamma_0) - 1)}. \quad \text{(B5)}$$

In the equation above $\gamma_0 = L/(2\pi\lambda)$ tends to zero. Taking the limit $\gamma_0 \to 0$ gives

$$term_0 = \frac{\sin\theta}{2} \left[\frac{1}{\pi\gamma_0^2} + \frac{1}{3}\pi \left(1 - 6\left(\frac{R_1}{L}\right) + 6\left(\frac{R_1}{L}\right)^2 \right) \right]. \quad \text{(B6)}$$

Now the first term in the equation above is a constant (albeit infinite) independent of R_1 and R_2 and after dropping it we are left with the following expression:

$$term_0 = \frac{\sin\theta}{2} \left[\frac{1}{3}\pi \left(1 - 6\left(\frac{R_1}{L}\right) + 6\left(\frac{R_1}{L}\right)^2 \right) \right]. \quad \text{(B7)}$$

Eq. (B4) with with $\gamma_n = n\sin\theta$ together with Eq. (B7) constitute the required summation over a logarithmic potential under 2D periodic boundary conditions.

[1] M. Tinkham in *Introduction to Superconductivity*, McGraw-Hill, 1975.

[2] G. Blatter, M. V. Feigel'man, V. B. Geshkenbein, A. I. Larkin and V. M. Vinokur, Rev. Mod. Phys. **66**, 1125 (1994) and references therein.

[3] E. H. Brandt, Rep. Prog. Phys. **58**, 1465 (1995).

[4] H. Safar, P.L. Gammel, D.A. Huse, D. J. Bishop, J. P. Rice, and D. M. Ginsberg, Phys. Rev. Lett. **69**, 824 (1992).

[5] W. K. Kwok, S. Fleshler, U. Welp, V. M. Vinokur, J. Downey, G. W. Crabtree, and M. M. Miller, Phys. Rev. Lett. **69**, 3370 (1992).

[6] R. Cubitt, E. M. Forgan, G. Yang, S. L. Lee, D. M. Paul, H. M. Mook, M. Yethiraj, P. H. Kes, T. W. Li, A. A. Menovsky, Z. Tarnavski and K. Mortensen, Nature **365**, 407 (1993).

[7] E. Zeldov, D. Majer, M. Konczykowski, V. B. Geshkenbein, V. M. Vinokur, and H. Shtrikman, Nature **375**, 373 (1995).

[8] A. Schilling, R. A. Fisher, N. E. Phillips, U. Welp, D. Dasgupta, W. K. Kwok, and G. W. Crabtree, Nature **382**, 791 (1996).

[9] J. C. Martinez, S. H. Brongersma, A. Koshelev, B. Ivlev, P. H. Kes, R. P. Griessen, D. G. de Groot, Z. Tarnavski, and A. A. Menovsky, Phys. Rev. Lett. **69**, 2276 (1992).

[10] S.L. Lee, C.M. Aegerter, H. Keller, M. Willemin, B. Stauble-Pumpin, E.M. Forgan, S.H. Lloyd, G. Blatter, R. Cubitt, T.W. Li, and P. Kes, Phys. Rev. B **55**, 5666 (1997).

[11] M. B. Gaifullin, Y. Matsuda, N. Chikumoto, J. Shimoyama, and K. Kishio, Phys. Rev. Lett **84**, 2945 (2000).

[12] J. R. Clem, Phys. Rev. B **43**, 7837 (1991).

[13] H. Nordborg and G. Blatter, Phys. Rev. B **58**, 14556 (1998).

[14] D. R. Nelson, Phys. Rev. Lett. **60** , 1973 (1988).

[15] S. N. Artemenko and A. N. Kruglov, Phys. Lett. A **143**, 485 (1990).

[16] J. R. Clem, M. W. Coffey, and Z. Hao, Phys. Rev. B **44**, 2732 (1991).

[17] S. Ryu, S. Doniach, G. Deutscher, and A. Kapitulnik, Phys. Rev. Lett. **68**, 710 (1992); S. Ryu, Ph.D. Thesis, Stanford University (1995).

[18] G. Blatter, V. Geshkenbein, A. Larkin, and H. Nordborg, Phys. Rev. B **54**, 72 (1996).

[19] X. Hu, S. Miyashita, and M. Tachiki, Phys. Rev. Lett. **79**, 3498 (1997).

[20] X. Hu, S. Miyashita, and M. Tachiki, Phys. Rev. B **58**, 3438 (1998).

[21] A. E. Koshelev, Phys. Rev. B **56**, 11201 (1997).

[22] Y. Nonomura and X. Hu, Phys. Rev. Lett. **86**, 5140 (2001).

[23] P. Olsson and S. Teitel, Phys. Rev. Lett. **87**, 137001 (2001).

[24] S.-K. Chin, A. K. Nguyen, and A. Sudbo, Phys. Rev. B **59**, 14017 (1999).

[25] S. Tyagi and Y. Y. Goldschmidt, Phys. Rev. B **67**, 214501 (2003).

[26] C. J. Olson, G.T. Zimányi, A.B. Kolton, and N. Gronbech-Jensen, Phys. Rev. Lett. **85** , 5416 (2000).

[27] A.B. Kolton, D. Dominguez, C.J. Olson, and N. Gronbech-Jensen, Phys. Rev. B **62**, R14 657 (2000).

[28] C.J. Olson, C. Reichhardt, and V.M. Vinokur, Phys. Rev. B **64**, 140502 (2001).

[29] W. E. Lawrence and S. Doniach, in *Proceedings of LT 12, Kyoto,1970*, edited by E. Kanda (Keigaku, Tokyo, 1971),p. 361; S. Doniach, in *High Temperature Superconductivity, Proceedings*, edited by K. S. Bedell *et al.* (Addison-Wesley, Redwood City, 1989), p. 406.

[30] M. V. Feigel'man, V. B. Geshkenbein and A. I. Larkin, Physica C **167**, 177 (1990).

[31] M. P. Allen and D. J. Tildesley, *Computer Simulation of Liquids*(Clarendon Press, Oxford, 1987).

[32] D. M. Ceperley, Rev. Mod. Phys. **67**, 279 (1995).

[33] S. Sengupta, C. Dasgupta, H. R. Krishnamurthy, G. I. Menon, and T. V. Ramakrishnan, Phys. Rev. Lett. **67**, 3444 (1991).

[34] W. R. Magro and D. M. Ceperley, Phys. Rev. B **48**, 411 (1993).

[35] O. Waldmann, F. Steinmeyer, P.Muller, J. Neumeier, F. X. Regi, H. Savary and J. Schneck, Phys, Rev. B **53**, 11825 (1996).

[36] G. W. Crabtree and D. R. Nelson, Physics Today **50**, 38 (April 1997).

[37] M. J. W. Dodgson, A. E. Koshelev, V. B. Geshkenbein, and G. Blatter, Phys. Rev. Lett. **84**, 2698 (2000).

[38] H. Fangohr, A. E. Koshelev, and M. J. W. Dodgson, Phys. Rev. B **67**, 174508 (2003)

[39] B. Khaykovich, M. Konczykowski, K. Teitelbaum, E. Zeldov, H. Shtrikman, and M. Rappaport, Phys. Rev. B **57**, R14088 (1998).

[40] D. Majer, E. Zeldov, and M. Konczykowski, Phys. Rev. Lett. **75**, 1166 (1995).

[41] G. I. Menon and C. Dasgupta, Phys. Rev. Lett. **73** , 1023 (1994).

[42] Y. Y. Goldschmidt and S. Tyagi, in preparation (unpublished).